Orbital
The electronic journal of chemistry

the electronic journal of chemistry

Full Paper | http://dx.doi.org/10.17807/orbital

Zinc Niobate Hydrothermally Synthesized as a Catalyst for the Photodegradation of Organic Compounds

Josias R. V. Nascimento* [a], Bruna A. Perek [a], Alan F. Matsushita [a], João M. A. Leite [a], and Jarem R. Garcia [a]

Zinc Niobate $ZnNb_2O_6$ is a semiconductor compound that remains relatively unexplored for photocatalyst applications. In this work, we present a hydrothermal synthesis method that allows obtaining $ZnNb_2O_6$ with high surface area, nanometric size and high capacity for adsorption and degradation of dyes. Zinc niobate has a band gap of 3.36 eV and can be used as a photocatalyst when activated by ultra violet (UV) light, enabling the degradation of dyes and others organic compounds. Zinc niobate was tested as a photocatalyst for the degradation of methylene blue at different pH values and showed high dye degradation kinetics in both acidic and basic media.

Graphical abstract

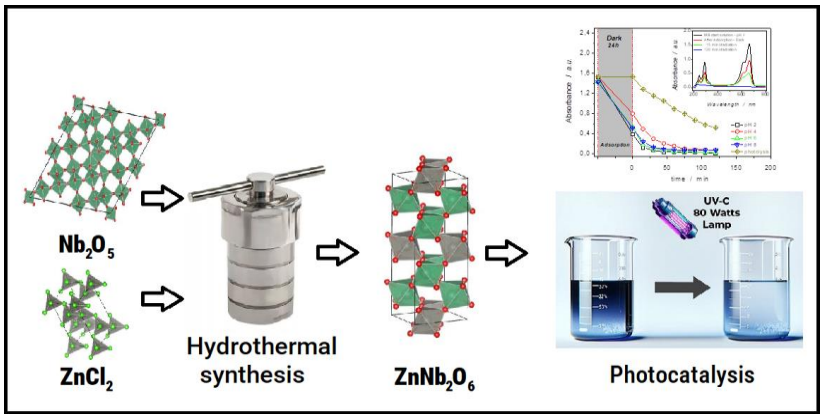

Keywords

Zinc Niobate
Catalyst,
Dye degradation
Niobium
Photocatalysis

Article history

Received 28 Jun 2024
Revised 16 Jan 2025
Accepted 18 Feb 2025
Available online 19 May 2025

Handling Editor: Sergio R. Lazaro

1. Introduction

The search for economic growth as a means of advancing society comes at a cost in terms of environmental degradation [1, 2]. This degradation is mainly manifesting in forms such as water and air pollution, depletion of natural resources, and climate change is evident in various forms. The unregulated discharge of numerous hazardous substances, including dyes, chemicals, heavy metals, organic solvents, petroleum products, and solid waste, poses a severe threat to environmental integrity.

Among these hazardous substances, synthetic dyes, widely utilized in various industrial processes, particularly in textile manufacturing, attract a significant concern [3]. Their presence in water systems poses a threat to aquatic life due to their toxicity and potential to induce mutations in organisms. Consequently, specific treatment methods are required to ensure their complete removal. Various chemical and physical processes, such as adsorption, precipitation, ultrafiltration, reverse osmosis, and flocculation, are employed to eliminate toxic substances, including synthetic dyes, from industrial effluents. However, these processes often generate significant amounts of sludge, leading to reduced operational lifetimes and increased maintenance

[a] Department of Chemistry, State University of Ponta Grossa (UEPG). Av. General Carlos Cavalcanti 4748 - Uvaranas, zip code 84030-900, Ponta Grossa, Paraná, Brazil. *Corresponding author. E-mail: **josiasvitor4@gmail.com**

costs [4]. Heterogeneous photocatalysis offers a promising approach to effectively remove a wide range of organic pollutants, including textile dyes, in a straightforward manner. This method involves the use of solid semiconductors, such as TiO_2, ZnO, and Fe_2O_3, along with light energy exceeding the band-gap energy of the semiconductor, to generate hydroxyl radicals (•OH), potent oxidants responsible for the mineralization of organic pollutants. Compared to conventional methods, heterogeneous photocatalysis offers the advantage of gradually breaking down contaminant molecules without leaving behind residual organic matter, thus eliminating the need for sludge disposal in landfills. Additionally, it has been shown to be a cost-effective alternative to biological treatment processes for water purification [5].

Niobium materials have been widely explored for various catalytic reactions, owing to their unique properties. Sodium niobate ($NaNbO_3$), for instance, a perovskite-structured n-type semiconductor composed of NbO_6 octahedra, exhibits remarkable photocatalytic activity, corrosion resistance, chemical stability, and non-toxicity. These properties make it a promising candidate for applications in solar fuel production and the removal of organic pollutants from water systems [6]. Similarly, disodium tetraniobium hendecaoxide ($Na_2Nb_4O_{11}$), a ceramic material belonging to the ferroelectric material family, demonstrates a monoclinic structure with distinctive dielectric properties. Studies have revealed its unique arrangement in layers comprising edge-sharing pentagonal Nb-O bipyramids alternating with layers of edge-sharing octahedra, underscoring its potential for various applications in materials science and catalysis [7].There are few works about of use of $ZnNb_2O_6$ as a photocatalyst. Wang et al., (2019) [8] used the $ZnNb_2O_6$ fiber for the reduction of nitrobenzene to produce selective aniline under near-UV light, with 95 % of conversion, 78% most efficient than Nb_2O_5, and 10% higher than ZnO. The photocatalytic capacity of $ZnNb_2O_6$ can also be used to produce hydrogen gas using the water splitting method, which can produce up to 23.6(±5) mmol h^{-1} g^{-1} in the presence of 20% methanol with the sacrificial agent [9].

The Zinc Niobate with the formula $ZnNb_2O_6$ is a ceramic semiconductor with a band gap of ~ 3.35 eV [8]. The $ZnNb_2O_6$ can be synthesized by hydrothermal method [8], Sol-gel [6], coprecipitation [10], solid-state method [11-13], and ball milling [14].

In this study we report methodology to produce zinc niobate using the hydrothermal method. The prepared material was structurally characterized by Field Emission Gun Scanning Electron Microscopy (FEG-SEM), X-Ray diffraction (XRD) and Brunauer-Emmett-Teller isotherm method (BET) measurements which revelled its crystallographic order nanometric microstructures and surface area. The Band Gap of the material was determined by UV-vis spectroscopy (UV-vis) measurement and the evaluation of the photocatalytic activity was carried out through degradation tests of the Methylene Blue Dye (MB), performed using the materials prepared. This evaluation was produced as a proof of concept intending to show the possibility application of the Zinc Niobate nanostructure as catalyst for photodegradation of organic pollutants.

2. Material and Methods

All the reagents were used received by the suppliers without further purification, niobium pentoxide with optical grade was kindly provided by Brazilian company CBMM Brazil (Companhia Brasileira de Metalurgia e Mineração), potassium hydroxide was purchased from Neon®, zinc chloride, hydrochloric acid, anhydrous ethanol and methylene blue dye with reagent grade were purchased from Sigma Aldrich®.

2.1 Synthesis of Zinc Niobate

The Zinc Niobate ($ZnNb_2O_6$) was prepared using a procedure adapted from *Y Chun et al 2018*. In the first step of the synthesis, 4.0 g of Nb_2O_5 was dispersed in 50 mL of KOH 4.0 mol L^{-1} and transferred to a PTFE (Polytetrafluoroethylene) sealed steel reactor, which was kept at 180°C for 12 h to the hydrothermal process. The clean solution of potassium niobate obtained was precipitated adding 30 mL of ethanol and the supernatant was discarded. The precipitate was dissolved again with 30mL of water and warmed at 90°C for 30 minutes. The solution of potassium niobate was neutralized using the hydrochloric acid solution 1.0 mol L^{-1} until pH 8. In a second step of the synthesis, a 50 mL of an aqueous solution containing 3.0 g of zinc chloride was slowly mixed with the solution of potassium niobate. The white suspension of zinc niobate ($ZnNb_2O_6$) was transferred to the same PTFE lined sealed steel reactor, which was kept at 180°C for 12 h to the hydrothermal process. The product obtained was filtered and washed with distilled water, dried in an oven at 60°C for 4 h and grinded using agate mortar.

2.2 Characterization

The $ZnNb_2O_6$ was characterized by Field Emission Gun Scanning Electron Microscopy (FEG-SEM) using a Tescan® Mira 3, by X-Ray diffraction (XRD) using a Rigaku® Ultima IV, by UV-Visible Diffuse Reflectance Spectroscopy (DRS) using a Varian® Cary 50 and by superficial area using a Brunauer-Emmett-Teller isotherm method (BET) (Quantachrome TouchWin™).

The FEG-SEM images were obtained at different magnification levels and prior to the acquisition, the samples were covered by a thin gold layer to avoid sample charging. The XRD patterns were obtained with a CuKα radiation (λ = 1.5418 Å), operated at 40 kV/30 mA. The diffraction patterns were recorded at scan rate of 1º (2θ) min^{-1} in the 10º < 120º (2θ) range. The DRS measurements were performed in the 200-800 nm range, employing the integration sphere diffuse reflectance attachment. The finely ground powder samples (~20 mg) were measured using solid barium sulphate ($BaSO_4$) standard as the baseline.

2.3. Photodegradation

The degradation of the solution of methylene blue 10.0 mg L^{-1} was carried out using a Lab-made UV-C reactor with an 80 Watts mercury lamp for 2 h. The concentration of the catalyst was 1.5 g L^{-1} of dye solution, kept in the dark with agitation for 24h of adsorption before the photodegradation. It was used 150 mL of dye solution and samples of 3 mL were automatically collected every 15 minutes. The pH of solutions was adjusted to 2, 4, 6, and 8 using phosphoric acid and NaOH solutions, both with concentration of 0.5 mol L^{-1}. The discoloration of the MB solution was tracked by UV-vis measurement and the dye colour fading was followed by the maximum of absorption of the band centered at *c.a.* 660 nm.

3. Results and Discussion

The prepared material morphology was observed using FEG-SEM (Figure 1 A and B) These micrographs indicate that the bulk material consists of highly agglomerated particles, with spherical nanosized particles with average size around 100 nm. Figure 1*C* shows the relative compositional analysis obtained by EDX. It is possible to observe that the material is composed only by oxygen, zinc and niobium. Figure 1C also shows the EDX mapping relative to Nb and Zn, which indicates that these elements are well distributed throughout the material.

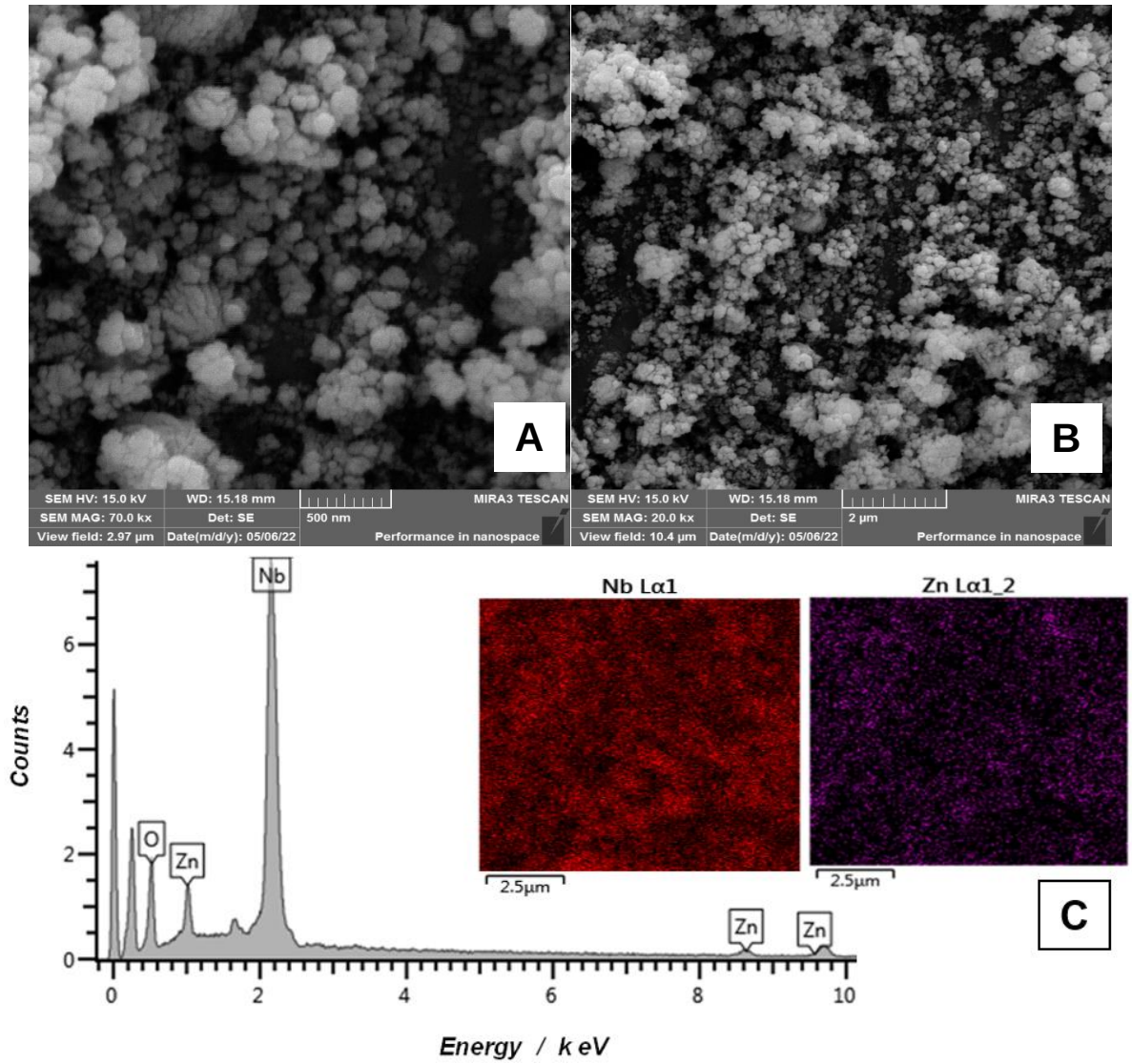

Fig. 1. Field Emission Gun Scanning Electron Microscopy (FEG-SEM) image of the zinc niobate prepared using hydrothermal technique at different magnification: ***a)*** at 20 *k***x**, ***b)*** 70 *k***x** and ***c)*** EDX relative compositional analysis and mapping relative to Nb and Zn.

The crystal structure of the material was obtained by XRD measurements. Figure 2 shows the XRD patterns of the material obtained, it is possible to observe the main diffraction peaks it 2θ values corresponding to the indexed reflecting planes (*hkl*) as follow: 24.2° (*310*), 30.3° (*311*), 35.6° (*020*), 38.1° (*510*), 40.6° (*002*), 51.6° (*330*), 53.2° (*621*), 63.7° (*332*). The result obtained matched with the JCP DS file numbers 76–182, related to the structure $ZnNb_2O_6$ [15] though, the broad peaks and the low maximum intensity of the peaks indicated that the material was obtained with a low degree of crystallinity, which is a common aspect in hydrothermal produced structures. According to Ücker et al., (2021)[16] , the Nb_2O_5 produced by hydrothermal method exhibits a high surface area and a poorly organized structure, which enhances its catalytic performance. In contrast, high temperature treatments cause pore coalescence and crystal growth, reducing the surface area and photocatalytic efficiency. Similarly, the low crystallinity of $ZnNb_2O_6$ produced by hydrothermal method can also contribute to improving its catalytic capacity."

The observed peaks can be well indexed by the columbite-type orthorhombic structure with space group ***P****bcn*. This structure is composed of two different octahedral units ZnO_6 and NbO_6 where the divalent Zn^{2+} and pentavalent Nb^{5+} cations occupy two distinct sites. The NbO_6 octahedra are connected via edge-sharing, thereby forming zig-zag chains along the c-axis. These chains are connected along (1 0 0) through the ZnO_6 octahedral units by corner-sharing [17] A crystal model for the product $ZnNb_2O_6$, obtained from the

Materials Project [18], is shown in Figure 2, alongside the XRD plot.

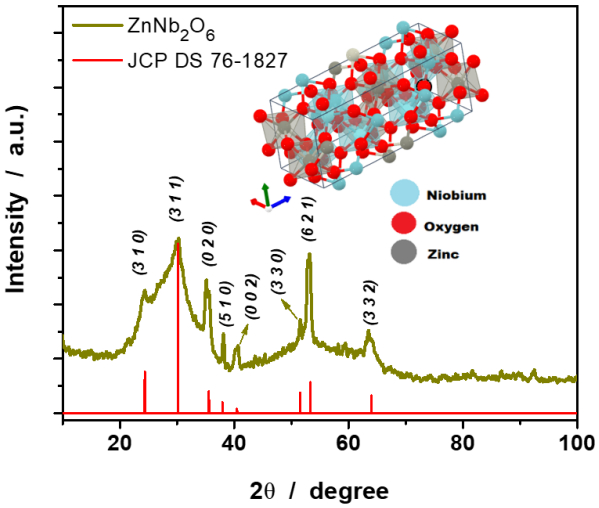

Fig. 2. XRD patterns of the $ZnNb_2O_6$ obtained by hydrothermal process. It is also shown the JCP DS file numbers 76–1827 structure and an insert with the simulated structure of the columbite-type orthorhombic Zinc Niobate.

The optical and electronic characterization of the $ZnNb_2O_6$ nanostructure, produced with hydrothermal procedure, was performed by UV-vis Diffuse Reflectance Spectroscopy (DRS) (Figure 3). The DRS spectra demonstrated that the material produced sharper reflection steep edges in a region at about 380 nm. The region of absorption (represented by the decrease in the reflection percentage) between 380 and 200 nm was not structured. The quantitative interpretation of the observations presented above can be done with the estimation of the *Eg* energy value for the studied material. This value was calculated using Tauc's plot relationship, which relates the absorption coefficient and incident photon energy of the $ZnNb_2O_6$ which, for the diffuse reflection of nanoparticles, is given by the Kubelka–Munk function [19]. In this case, the Tauc's plot was constructed with the square root of the Kubelka–Munk function multiplied by the photon energy and plotted against the photon energy, so the energy was estimated by the intercept of the linear region of the Tauc's plot to the *x* axis [19]. The *Eg* value obtained for $ZnNb_2O_6$ was calculated as 3.36 eV, value close to 3.35 eV found by of Costa et al., (2020) [20] and lower than 3.95 eV found by de Y Chun et al., (2018) [21].

The optical/electronic characterization of the $ZnNb_2O_6$ indicates the possibility of application of this nanostructure as a photocatalyst for organic molecules degradation under ultraviolet irradiation.

As a proof of concept of this possibility, the photocatalytic ability of the produced $ZnNb_2O_6$ was evaluated for the degradation of the dye Methylene Blue (MB), under irradiation of a high-pressure mercury vapor lamp. Figure 4 shows the decline in the visible light absorbance of the dye solution with time of irradiation. This decrease in light absorption was ascribed to the MB discoloration but cannot be recognized as a full degradation of the dye. The process of MB colour fading in solution when oxidizing species are present starts with the degradation of dye chromophore produced by broken the C–S and C–N bonds present at the central heterocycle moiety [22, 23]. In this way, the dye removal process was monitored considering the discoloration of the dye solution, followed by UV-vis spectroscopy.

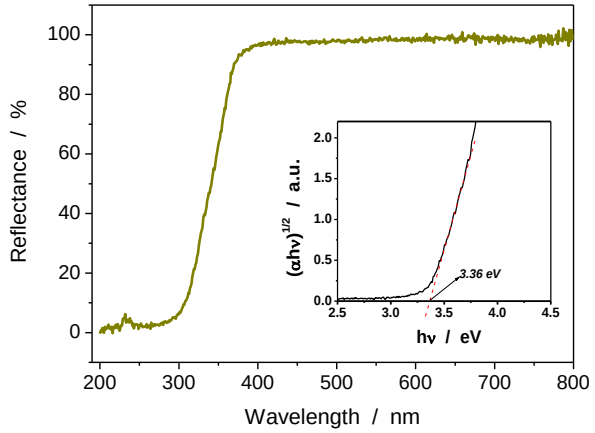

Fig. 3. DRS spectra of the $ZnNb_2O_6$ nanostructures obtained by hydrothermal procedure and an insert showing the Tauc's plot and the intercept of the linear region to the *x* axis and the estimation of *Eg* energy for the material.

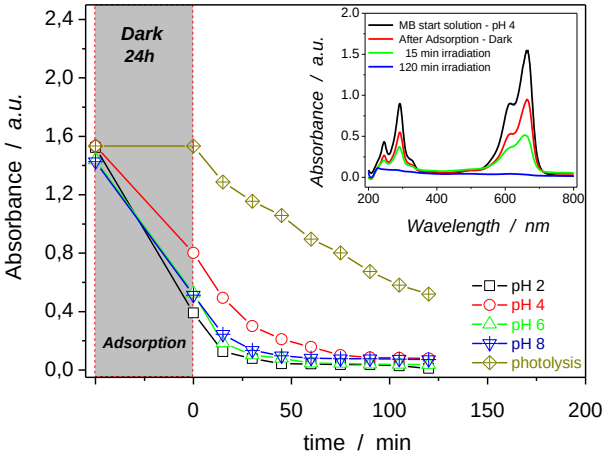

Fig.4. Discoloration of Methylene blue (MB) solution with ultraviolet irradiation time in the presence of the $ZnNb_2O_6$ at different pHs. It is also shown the discoloration produced without the presence of catalyst (photolysis). The irradiation starts after 24 h of adsorption, when the samples were kept in dark. The insert of the figure shows the UV–vis spectra of the MB solutions after different treatment times at pH 4.

Before the system dye/catalyst be submitted to light irradiation, it was kept in dark during 24h to evaluate the adsorption capability of the catalyst surface. As can be seen in Figure 4, the adsorption process decreases the dye absorbance in more of 50 % in all the pH studied. To evaluate the capacity of adsorption the surface area of the catalyst was obtained by BET and it was found a value of 68.7 $m^2\ g^{-1}$ which is like 75 $m^2\ g^{-1}$ found by Costa et al., (2020) for the $ZnNb_2O_6$ obtained by solid state method [24].

The influence of pH of the medium on the catalytic MB discoloration was evaluated since the performance of a photocatalyst is deeply influenced by pH levels. This parameter directly impacts the surface charge properties of the photocatalyst, affecting the oxidation potential of reactions. Moreover, it alters the double layer of the solid electrolyte interface, thereby influencing the sorption-desorption process and the separation of photogenerated h^+/e^- pairs on the semiconductor photocatalyst's surface. pH not only plays a crucial role in hydroxyl radicals generation

but also impacts the charge on the photocatalyst particles and the positions of valence and conduction bands [25, 26]. Research indicates that the photocatalytic degradation of MB intensifies in solution at alkaline pH. This phenomenon is linked to the positively charged nature of MB, since the negative charge of the catalyst surface thrives in alkaline environments, enhancing its adsorption and thereby boosting photocatalytic degradation [27].

The $ZnNb_2O_6$ is activated under ultraviolet when photons with energy equal to or greater than its band gap strike the material, resulting in the generation of an electron-hole pair. This pair exhibit high oxidative and reductive capacities, enabling reactions with adsorbed oxygen and water molecules to produce reactive species such as •OH radicals. These radicals are highly efficient in oxidizing organic compounds like methylene blue (MB), breaking them down into intermediate products and eventually converting them into CO_2 and H_2O [16, 27, [28]. The reactions involved can be represented by the following equations:

$$ZnNb_2O_6 + h\nu \rightarrow ZnNb_2O_6 + (e^-) + (h^+) \quad (1)$$

$$(e^-) + O_2 \rightarrow O_2^{\bullet-} \quad (2)$$

$$(h^+) + H_2O \rightarrow H^+ + \bullet OH \quad (3)$$

$$2e^- + O_2 + 2H^+ \rightarrow H_2O_2 \quad (4)$$

$$O_2^{\bullet-} + O_2^{\bullet-} + 2H^+ \rightarrow H_2O_2 + O_2 \quad (5)$$

$$H_2O_2 + e^- \rightarrow \bullet OH + OH^- \quad (6)$$

$$H_2O_2 + O_2^{\bullet-} \rightarrow \bullet OH + OH^- + O_2 \quad (7)$$

$$H_2O_2 + hv \rightarrow 2\bullet OH \quad (8)$$

$$MB + \bullet OH \rightarrow \text{intermediate products} \rightarrow CO_2 + H_2O \quad (9)$$

The stoichiometric equations of the total oxidation of MB is: [27].

$$C_{16}H_{18}N_3S^+ + \frac{51}{2}O_2 \rightarrow 16CO_2 + 3NO_3^- + SO_4^{2-} + 6H^+ + 6H_2O \quad (10)$$

The complete photodegradation of methylene blue is a complex process but can be simplified into a few key steps. Initially, the molecule are oxidized by •OH radicals, leading to the cleavage of N-CH_3, C-S and C-N bonds, which form intermediate products such as formaldehyde and formic acid. Aromatic rings in methylene blue are converted into compounds like 2,5-diaminobenzenesulfonic acid and 4-aminocatechol. The 2,5-diaminobenzenesulfonic acid can further react with formaldehyde to produce benzothiazole [22]. These intermediates can be further oxidized by •OH radicals to form CO_2 and H_2O, among other products like NO_3^- and SO_4^{2-} [22, 23].

However, the behaviour of the MB degradation catalysed by the $ZnNb_2O_6$ produced demonstrated that the rate of discoloration does not depends strongly with pH. It is possible to observe in Figure 4 that de rate of discoloration is higher for pH 2. The rate decreases at pH 4 but increase again at pH 6 and 8, to values close to the observed for pH 2. The superior performance of photocatalysis at pH 2 can be attributed to the presence of H^+, which reacts with O_2 and $O_2^{\bullet-}$ radicals producing H_2O_2, (equations 4 and 5), H_2O_2, in turn, decomposes under ultraviolet light, generating highly reactive •OH radicals that significantly enhance the photocatalytic degradation process. To find appropriates kinetics parameters for the photocatalytic degradation of MB, the concentration versus time data obtained for different pH evaluated were used to fit the integral forms of the pseudo first order (Lagergren's rate law).

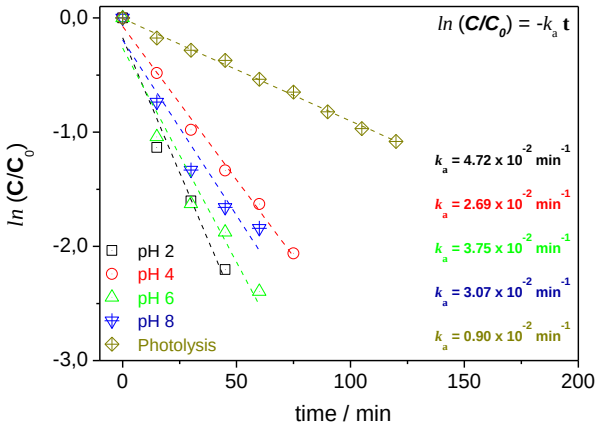

Fig. 5. Kinetic values obtained for each experiment with different pH values and also photolysis.

It could be seen that the apparent rate constant (k_a) for the MB photodegradation has similar values for the different pH, and the k_a for photolysis (degradation in the absence of the catalyst) is about 3-5 times lower than the ka obtained with the use of the catalyst.

It is interesting to notice that the obtained k_a values for photocatalytic decolouration of the MB are closed to the values reported in literature for the use of different catalyst, showing the potentials of using the reported material in dye degradation in wastewater treatment [29]. It is crucial to understand the kinetics of photocatalytic reactions and derive their rate laws to successfully implement them on a large scale.

The use of $ZnNb_2O_6$ as a photocatalyst offers several advantages compared to other niobate-based materials, mainly due to the low cost and abundance of the niobium mineral in Brazil. Additionally, $ZnNb_2O_6$ exhibits a high surface area and excellent photocatalytic activity. It can also be synthesized rapidly and at relatively low temperatures through the hydrothermal method, further enhancing its practicality and cost-effectiveness.

4. Conclusions

In this work, zinc niobate was successfully synthesized using niobium pentoxide as a precursor. The hydrothermal method enabled the production of a material with a high surface area, exhibiting excellent adsorption capacity and photocatalytic efficiency for the degradation of methylene blue. The influence of pH on the degradation rate was investigated, with the results showing that the degradation rate was highest at pH 2, 6, and 8. At these pH levels, over 95% of the dye was removed within two hours, compared to only 66% removed through photolysis under the same conditions. Zinc niobate demonstrated remarkable efficiency in the photodegradation process, highlighting its potential for the degradation of other organic compounds.

Acknowledgments

The author J.R.V. Nascimento thanks the National Council for Scientific and Technological Development of

Brazil for providing a scholarship, which was very important for the development of this work. The author also thanks the State University of Ponta Grossa and everyone who contributed directly or indirectly to the execution of this work.

Author Contributions

Author J.R.V. Nascimento was responsible for research, methodology, and writing. B.A. Perek was responsible for writing the review and visualization. A. F. Y. Matsushita was responsible for Formal Analysis and Validation. J.M.A. Leite was responsible for the use of Software and Conceptualization. J.R. Garcia was responsible for Project Administration, Supervision, Data Processing and Fund Acquisition.

References and Notes

[1] Priyadharsini, P.; SundarRajan, P.; Pavithra, K. G. *et al. J. Clean. Prod.* **2023**, *426*, 139180. [Crossref]

[2] Krishnan, A.; Swarnalal, A.; Das, D. *et al. J. Environ. Sci.* **2024**, *139*, 389. [Crossref]

[3] Mahmoud, M. A.; Alsehli, B. R.; Alotaibi, M. T. *et al. Environ. Sci. Pollut. Res. Int.* **2024**, *31*, 3466. [Crossref]

[4] Arkwa, J. B.; Oturan, N.; Acayanka, E. *et al. Environ. Chem. Lett.* **2019**, *17*, 473. [Crossref]

[5] Saeed, M.; Muneer, M.; ul Haq, A. *et al. Environ. Sci. Pollut. Res.* **2022**, *29*, 293. [Crossref]

[6] Hsiao, Y. J.; Fang, T. H.; Ji, L. W. *Mater. Lett.* **2010**, *64*, 2563. [Crossref]

[7] Kumari, N.; Gaurav, K.; Samdarshi, S. K.; Mohanty, K. *Sol. Energy Mater. Sol. Cells* **2020**, *208*, 110408. [Crossref]

[8] Wang, J.; Ge, Z.; Pei, L. *et al. Catal. Sci. Technol.* **2019**, *9*, 6681. [Crossref]

[9] Chun, Y.; Yue, M.; Jiang, P. *et al. RSC Adv.* **2018**, *8*, 13857. [Crossref]

[10] Navale, S. C.; Gaikwad, A. B.; Ravi, V. *Mater. Lett.* **2006**, *60*, 1047. [Crossref]

[11] Ngamjarurojana, A.; Khamman, O.; Yimnirun, R. *et al. Mater. Lett.* **2006**, *60*, 2867. [Crossref]

[12] Rajput, H.; Kwon, E. E.; Younis, S. A. *et al. Chem. Eng. J.* **2021**, *412*, 128612. [Crossref]

[13] Yang, J.; Yan, J. K.; Du, J. H. *et al. Mater. Sci. Forum* **2016**, *849*, 209. [Crossref]

[14] Kong, L. B.; Ma, J.; Huang, H. *et al. J. Alloys Compd.* **2002**, *347*, 308. [Crossref]

[15] Pakawanit, P.; Amonpattaratkit, P.; Yimnirun, R. *et al. Ferroelectr. Lett. Sect.* **2013**, *40*, 85. [Crossref]

[16] Ücker, C. L. *et al. Chem. Phys. Lett.* **2021**, *764*, 138271. [Crossref]

[17] Yang, H.; Zhang, S.; Yang, H. *et al. J. Am. Ceram. Soc.* **2019**, *102*, 5365. [Crossref]

[18] Jain, A.; Ong, S. P.; Hautier, G. *et al. APL Mater.* **2013**, *1*, 011002. [Crossref]

[19] Abdullahi, S. S.; Güner, S.; Koseoglu, Y. *et al. J. Niger. Assoc. Math. Phys.* **2016**, *35*, 241.

[20] Prado, A. G. S.; Bolzon, L. B.; Pedroso, C. P. *et al. Appl. Catal. B Environ.* **2008**, *82*, 219. [Crossref]

[21] Chun, Y.; Yue, M.; Jiang, P. *et al. RSC Adv.* **2018**, *8*, 13857. [Crossref]

[22] Teng, X.; Li, J.; Wang, Z. *et al. RSC Adv.* **2020**, *10*, 24712. [Crossref]

[23] Wang, Q.; Tian, S.; Cun, J. *et al. Desalin. Water Treat.* **2014**, *51*, 5821. [Crossref]

[24] Pereira da Costa, G.; Rafael, R. A.; Soares, J. C. S. *et al. Catal. Today* **2020**, *344*, 240. [Crossref]

[25] Khan, I.; Saeed, K.; Ali, N. *et al. J. Environ. Chem. Eng.* **2020**, *8*. [Crossref]

[26] Rauf, M. A.; Ashraf, S. S. *Chem. Eng. J.* **2009**, *151*, 10. [Crossref]

[27] Lachheb, H.; Puzenat, E.; Houas, A. *et al. Appl. Catal. B Environ.* **2002**, *39*, 75. [Crossref]

[28] Wu, W.; Liang, S.; Ding, Z. *et al. J. Sol-Gel Sci. Technol.* **2012**, *61*, 570. [Crossref]

[29] Din, M. I.; Khalid, R.; Najeeb, J. *et al. J. Clean. Prod.* **2021**, *298*, 126567. [Crossref]

How to cite this article

Nascimento, J. R. V.; Perek, B. A.; Matsushita, A. F.; Leite, J. M. A.; Garcia, J. R. *Orbital: Electron. J. Chem.* **2025**, *17*, 247. DOI: http://dx.doi.org/10.17807/orbital.v17i2.21444